MOLECULAR SIMULATION OF THE ADSORPTION OF SEAWATER SALTS ON A NEGATIVELY CHARGED QUARTZ SURFACE

[1]GONZALO QUEZADA, [2]PEDRO G. TOLEDO

[1,2]Chemical Engineering Department and Surface Analysis Laboratory, University of Concepción, PO Box 160-C, Concepción, Chile
E-mail: [1]gonzaloquezada@udec.cl, [2]petoledo@udec.cl

Abstract— Molecular dynamics simulations of the (1001) surface of α-quartz interacting with aqueous solutions of different seawater salts are performed with the CLAYFF force field modified to describe the negative charging of the quartz surface. Results include cation density profiles and adsorption maps on the quartz surface. Results are compared with literature data. The adsorbed amount of cations decreases as the cation valence increases. For a series with the same valence the adsorbed amount decreases as the size of the bare cation increases, except for Li and Mg, and presumably Al. The latter cations are absorbed in their hydrated form with their hydration layers almost intact.

Index Terms— Adsorption, Seawater, Force field, Molecular simulation.

I. INTRODUCTION

Quartz is the second most common mineral in the earth's crust. α-Quartz (α-SiO2) is a crystalline form of silicon dioxide constituting about 20% of the Earth's exposed crust. The interface quartz/water is of great interest for a number of applications including geological [1-4], biological [5,6] and technological [7,8]. The subject is central in particular for the mining industry, the scarcity of fresh water has pushed this industry to use seawater, as such or partially desalinated. Mineral concentration typically involves separating the accompanying silicon dioxide (in all its forms), the presence of seawater salts can severely affect such separation. Thus, there is great need to improve our understanding about the impact of seawater salts, in particular the effect of electrolytes in the quartz-water interface [9-12]. Experimental work with monovalent salts show higher adsorption of the least hydrated cations on silica at high pH (see for instance [13-14]). Theoretical work based on molecular simulation of the quartz-water interface has been instrumental in unveiling the different interactions and mechanism operating there (see for instance [15-20]). Here we study the quartz-water interface in the presence of salts from seawater, monovalent, divalent and trivalent, via molecular dynamics and a robust force field. In particular we study the adsorption of nine sea water salts on quartz (1001) surface properly deprotonated..

II. METHODOLOGY

Here we used the general force field, CLAYFF [15], for the simulation of the interaction of α-quartz with aqueous solutions of several metal chloride salts with the metal cation a monovalent, Li, Na, K, Rb, Cs, divalent, Mg, Ca, Sr, or trivalent, Al, cation. The form of quartz is hexagonal prism, one of the most important and abundant crystallographic forms in quartz, with Miller-Bravais indices (1010). To incorporate deprotonation of interfacial silanol groups, that is, to change the quartz surface charge, we used a recently modified CLAYFF force field [20]. We used a slab of α-quartz with length Lx = 5.8992 nm, width Ly = 4.1271 nm, and thickness Lz = 1.1408 nm (corresponding to six atomic layers), the slab is periodic in the x and y directions, and the liquid solution is periodic in the three Cartesian coordinates. Quartz surface charge density is -0.12 C/m2 in the x-y plane corresponding to 18 deprotonated silanol groups distributed in a 3 × 6 array and a pH of 11 [20]. To describe the water and hydroxyl behavior we used the SPC/E water model [21]. For the ion-oxygen interactions we used the 12-6 LJ potential and a Coulombic term with recently updated parameters [23-24] which accurately reproduce ion-oxygen distance (IOD) and ion hydration free energy (HFE). The latter parameters were developed for the SPC/E water model with Lorentz-Berthelot mixing rules. For the simulations we used the GROMACS 5.0.2 software package run on NVIDIA graphic processing units to parallelize calculations and post-processing. The cut-off distance was 1.2 nm for the electrostatic and van der Waals potentials. The particle mesh Ewald (PME) algorithm was used to treat the long-range correction for electrostatic interactions [25]. Ions were placed in the system randomly keeping a distance of 0.8 nm between them and 1.0 nm from the quartz surface to a concentration of 0.5 M, and then the gaps were filled with water up to the density of liquid water at 300 K. First, the initial energy of the system was minimized by using a steepest descent integrator, followed by an equilibration stage of 0.1 ns run with the ions fixed in their positions in a NVT ensemble, in this stage ions develop their hydration layers. Finally, the ions were set free and a NVT production stage was run for 40 ns with an integration step of 2 fs, data was

collected every 1 ps. We used a modified Beredsen thermostat to maintain the temperature during the simulation [26].

III. RESULTS

Using the notation from ^{29}Si solid-state NMR spectroscopy, the quartz (1010) surface contains only Q^3 silica functional groups (see also the work of Skelton et al. [18]) for the quartz (1011) surface) where the superindex denotes the number of Si units attached via oxygen to an individual silicon atom. The Q^3 groups are connected to the quartz surface by means of three siloxane (Si-O-Si) bonds; the latter are the first to break when dissolution begins. The Q^3 groups appear as silanol (Si-O-H) groups above the surface, with some higher than others forming a sinuous smooth surface; the former are referred to as outer silanol groups, they are likely to be deprotonated, and the latter are referred to as inner silanol groups, that remain neutral [18,20]. The zero level at the quartz/solution interface was defined as the plane through the centers of mass of the outer silanol groups. Axial density profiles in the aqueous solution are defined from this zero level. Figure 1 shows axial number density profiles for all the cations considered. The results are shown separately for monovalent, divalent and trivalent cations. The profiles for the monovalent ions show that the cations are adsorbed into two layers at an oxygen-cation distance which is less than the sum of their radii indicating that the cations are not located orthogonal to the charged oxygens but rather in its neighborhood. This means that cations slightly penetrate the surface of the quartz in the depressions marked by the inner silanol groups. For all cations the first adsorbed layer is denser than the second. Definitely all monovalent cations, other than Li, rearrange their hydration layers to be adsorbed as bare ions. For Li is harder to shed the hydration layer and so, despite being the smallest cation of the monovalent series, the peak corresponding to the first adsorbed Li layer shows a distance comparable to that of Cs, which is a ~2.5 time bigger. This means that Li is not adsorbed totally free of its hydration layer and also that due to its higher charge density Li is adsorbed more orthogonal to the oxygen than the other cations of the series. This view is supported by the adsorption maps in Figure 2 showing that Li adsorbs, at least in the first layer, more collinearly with oxygen in the *z* direction than the other cations. In contrast, for the other cations, the adsorption maps for the first layer show clearly that adsorption occurs in the vicinity of the outer deprotonated silanol, the surface distribution of cations is more uniform revealing a repeating pattern: adsorption of cations is also promoted by inner silanol groups. The adsorption maps for the second adsorbed layer for all cations show that adsorption is less dense but more widespread, from Cs to Li. The profiles for the divalent ions in Figure 1 show that the cations are adsorbed according to different patterns. Mg is adsorbed in two layers with a third intercalated, the first layer concentrates almost all the adsorbed Mg; Ca is adsorbed in two layers with the first denser than the second; and Sr also is adsorbed is two layers but the second is the denser. Oxygen-cation distances in Figure 1 reveal that Mg is adsorbed fully hydrated, and Ca and Sr rearrange their hydration layer to be adsorbed closer to the quartz surface but is Ca, due to its higher charge density compare to Sr, which adsorbs more closely and in greater amount.

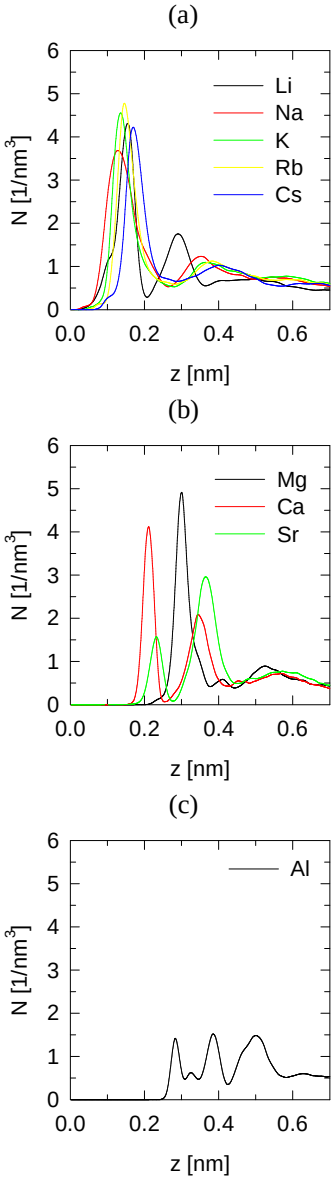


Figure 1 Axial number density profiles for (a) monovalent (b) divalent (c) trivalent cations at the (1010) surface of quartz. Charge density is -0.12 C/cm2. Each atom is scaled by its atomic size. Reference distance is from the center of mass of the oxygen in deprotonated outer silanol groups.

This view is supported by the adsorption maps in Figure 2 showing that Mg adsorbs, mostly in the first layer, around de oxygen. The hydration layer shields the electrical charge in the Mg and therefore prevents a

better alignment with the oxygen along the *z* axis. In the second layer Mg adsorbs in a very small amount but well distributed. The adsorption map for the intercalated layer is not shown in Figure 2. According to Figure 2 Ca adsorbs, at least in the first layer, collinearly with the oxygen along the z-axis which is likely due to the rearrangement of the hydration layer for a closer adsorption of Ca to the quartz surface. In the second layer Ca adsorbs in a significant amount and somewhat better distributed. The difference between Mg and Ca is that the first retains its hydration layer but the second only partially.

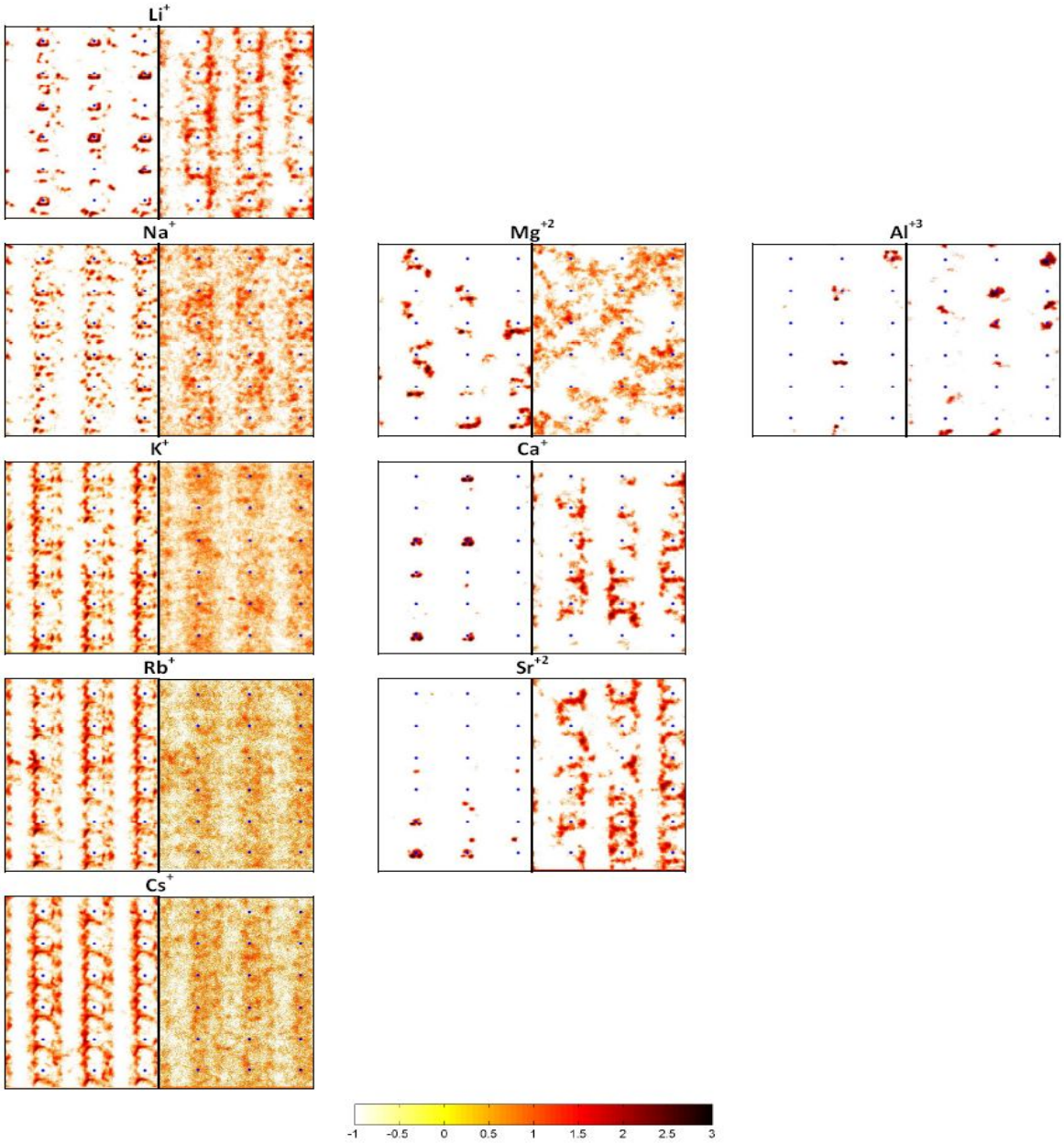


Figure 2 Adsorption density maps [1/nm3] for all the cations on the (1010) surface of quartz. Left maps correspond to the first layer (first peak in Figure 1), some bottom maps correspond to the second layer (second peak in Figure 1) for all the monovalent cations plus Ca and Sr, and some other bottom maps correspond to the third layer (third peak in Figure 1) for Mg and Al. Charge density is -0.12 C/cm2. The blue solid circles represent the center of mass of deprotenated surface oxygens. Color maps are in logaritmic scale.

Figure 2 shows that Sr adsorbs in very small amount in the first layer and a significantly greater amount in the second layer, in the latter adsorption is better distributed than for instance Ca. The profiles for the trivalent ion in Figure 1 show that Al is adsorbed in four layers with the second corresponding to an intercalated layer of low density. Oxygen-Al distances in Figure 1 reveal that Al is adsorbed fully hydrated with more than one water layer. This view is supported by the adsorption maps in Figure 2 showing that Al adsorbs, at least in the first layer, around de oxygen. As in the case of Mg, the hydration layer shields the electrical charge in the Al preventing a better alignment with the oxygen along the *z* axis. In the third

layer Al adsorbs in a greater amount and better distributed. The adsorption map for the intercalated layer and the fourth layer are not shown in Figure 2.
This view is supported by the adsorption maps in Figure 2 showing that Mg adsorbs, mostly in the first layer, around de oxygen. The hydration layer shields the electrical charge in the Mg and therefore prevents a better alignment with the oxygen along the z axis. In the second layer Mg adsorbs in a very small amount but well distributed. The adsorption map for the intercalated layer is not shown in Figure 2. According to Figure 2 Ca adsorbs, at least in the first layer, collinearly with the oxygen along the z-axis which is likely due to the rearrangement of the hydration layer for a closer adsorption of Ca to the quartz surface. In the second layer Ca adsorbs in a significant amount and somewhat better distributed. The difference between Mg and Ca is that the first retains its hydration layer but the second only partially. Figure 2 shows that Sr adsorbs in very small amount in the first layer and a significantly greater amount in the second layer, in the latter adsorption is better distributed than for instance Ca. The profiles for the trivalent ion in Figure 1 show that Al is adsorbed in four layers with the second corresponding to an intercalated layer of low density. Oxygen-Al distances in Figure 1 reveal that Al is adsorbed fully hydrated with more than one water layer. This view is supported by the adsorption maps in Figure 2 showing that Al adsorbs, at least in the first layer, around de oxygen. As in the case of Mg, the hydration layer shields the electrical charge in the Al preventing a better alignment with the oxygen along the z axis. In the third layer Al adsorbs in a greater amount and better distributed. The adsorption map for the intercalated layer and the fourth layer are not shown in Figure 2.

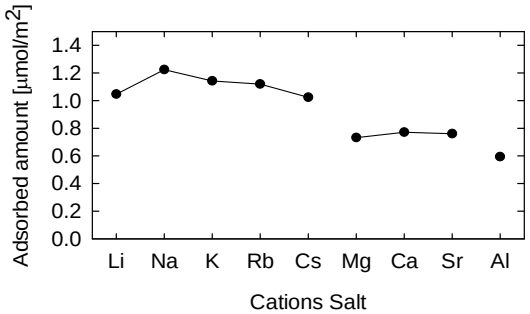


Figure 3 Amount of cations adsorbed on the (1010) surface of quartz. Charge density is -0.12 C/cm^2.

Figure 1 shows the total amount of cations adsorbed on the (1010) surface of quartz. The amount is calculated from Figure 1 by integrating over the interval 0 to 0.6 nm. Results for Na, Rb and Sr are similar to those of Kroutil et al. [20] for a surface charge density of -0.12 [C/m^2]. As expected, the adsorbed amount of cations decreases as the cation valence increases. For a series with the same valence the adsorbed amount decreases as the size of the bare cation increases, except for Li and Mg, and presumably Al. For the latter cations, the smallest in their series, the adsorbed amount decreases instead of increasing. However, one must consider that these cations are absorbed in their hydrated form with their hydration layers almost intact and therefore their effective size is much larger.

CONCLUSION

Monovalent actions are adsorbed into two layers at an oxygen-cation distance which is less than the sum of their radii; this means that monovalent cations slightly penetrate the surface of the quartz. For all cations the first adsorbed layer is denser than the second. Definitely all monovalent cations, other than Li, rearrange their hydration layers to be adsorbed as bare ions. Li is not adsorbed totally free of its hydration layer. Mg is adsorbed in two layers with a third intercalated, the first layer concentrates almost all the adsorbed Mg; Ca and Sr are adsorbed in two layers. Oxygen-cation distances reveal that Mg is adsorbed fully hydrated, and Ca and Sr rearrange their hydration layer to be adsorbed closer to the quartz surface. Al is adsorbed in four layers with the second corresponding to an intercalated layer of low density. Oxygen-Al distances reveal that Al is adsorbed fully hydrated with more than one water layer. The adsorbed amount of cations decreases as the cation valence increases. For a series with the same valence the adsorbed amount decreases as the size of the bare cation increases, except for Li and Mg, and presumably Al. For the latter cations, the smallest in their series, the adsorbed amount decreases instead of increasing. However, one must consider that these cations are absorbed in their hydrated form with their hydration layers almost intact and therefore their effective size is much larger.

ACKNOWLEDGEMENT

GQ thanks University of Concepción and CONICYT-Chile for graduate student fellowships. We thank Centro CRHIAM Project Conicyt/Fondap-15130015 and Red Doctoral REDOC.CTA, MINEDUC Grant UCO1202 for financial support.

REFERENCES

[1] Yang, X.-S. (2001). A unified approach to mechanical compaction, pressure solution, mineral reactions and the temperature distribution in hydrocarbon basins. Tectonophysics, 330 (1−2), 141−151.
[2] Newton, R. C.; Manning, C. E. (2008). Thermodynamics of SiO2−H2O fluid near the upper critical end point from quartz

solubility measurements at 10 Kbar. Earth Planet. Sci. Lett., 274 (1−2), 241−249.

[3] Koretsky, C. M.; Sverjensky, D. A.; Salisbury, J. W.; D'Aria, D. M. (1997). Detection of surface hydroxyl species on quartz, Γ-alumina, and feldspars using diffuse reflectance infrared spectroscopy. Geochim. Cosmochim. Acta, 61 (11), 2193−2210.

[4] Schulz, M. S.; White, A. F. (1999). Chemical weathering in a tropical watershed, Luquillo Mountains, Puerto Rico III: Quartz dissolution rates. Geochim. Cosmochim. Acta, 63 (3−4), 337−350.

[5] Tamerler, C.; Kacar, T.; Sahin, D.; Fong, H.; Sarikaya, M. (2007). Genetically engineered polypeptides for Inorganics: A utility in biological materials science and engineering. Mater. Sci. Eng., 27 (3), 558−564.

[6] Sano, K. -I.; Sasaki, H.; Shiba, K. (2005). Specificity and biomineralization activities of Ti-binding peptide-1 (TBP-1). Langmuir, 21 (7), 3090−3095.

[7] Papakonstantinou, P.; Vainos, N.; Fotakis, C. (1999). Microfabrication by UV femtosecond laser ablation of Pt, Cr and Indium oxide thin films. Appl. Surf. Sci., 151 (3−4), 159−170.

[8] Pinto, E. M.; Gouveia-Caridade, C.; Soares, D. M.; Brett, C. M. A. (2009). Electrochemical and surface characterization of carbon-film-coated piezoelectric quartz crystals. Appl. Surf. Sci., 255 (18), 8084−8090.

[9] Castro, S. (2012). Challenges in flotation of Cu-Mo sulfide ores in sea water. In Water in Mineral Processing–Proc. of the First International Symposium (J. Drelich, Ed.), SME (pp. 29-40).

[10] Castro, S.; Toledo, P.; Laskowski, J. S. (2012). Foaming properties of flotation frothers at high electrolyte concentrations. In Water in Mineral Processing–Proc. of the First International Symposium (J. Drelich, ed.), SME (pp. 51-60).

[11] Jeldres, R. I.; Toledo, P. G.; Stickland, A. D.; Usher, S. P.; Scales, P. J. (2014). Impact of seawater salts on the viscoelastic behavior of flocculated mineral suspensions. Colloids and Surfaces A: Physicochemical and Engineering Aspects, 461, 295-302.

[12] Goñi C.; Jeldres R. I.; Toledo P. G.; Stickland A. D.; Scales, P.J. 2015. A non-linear viscoelastic model for sediments flocculated in the presence of seawater salts, Colloids and Surfaces A, 482, 500–506.

[13] Colic, M.; Fisher, M. L.; Franks, G. V. (1998). Influence of ion size on short-range repulsive forces between silica surfaces. Langmuir, 14(21), 6107-6112.

[14] Franks, G. V. (2002). Zeta potentials and yield stresses of silica suspensions in concentrated monovalent electrolytes: isoelectric point shift and additional attraction. Journal of Colloid and Interface Science, 249(1), 44-51.

[15] Cygan, R. T.; Liang, J. J.; Kalinichev, A. G. (2004). Molecular models of hydroxide, oxyhydroxide, and clay phases and the development of a general force field. The Journal of Physical Chemistry B, 108(4), 1255-1266.

[16] Notman, R.; Walsh, T. R. (2009). Molecular dynamics studies of the interactions of water and amino acid analogues with quartz surfaces. Langmuir, 25(3), 1638-1644.

[17] Butenuth, A.; Moras, G.; Schneider, J.; Koleini, M.; Köppen, S.; Meißner, R.; Ciacchi, L. C. (2012). Ab initio derived force-field parameters for molecular dynamics simulations of deprotonated amorphous-SiO2/water interfaces. Physica Status Solidi (b), 249(2), 292-305.

[18] Skelton, A. A.; Fenter, P.; Kubicki, J. D.; Wesolowski, D. J.; Cummings, P. T. (2011). Simulations of the quartz(1011)/water interface: A comparison of classical force fields, ab initio molecular dynamics, and X-Ray reflectivity experiments. J. Phys. Chem. C 2011, 115 (5), 2076−2088.

[19] Emami, F. S.; Puddu, V.; Berry, R. J.; Varshney, V.; Patwardhan, S. V.; Perry, C. C.; Heinz, H. (2014). Force field and a surface model database for silica to simulate interfacial properties in atomic resolution. Chemistry of Materials, 26(8), 2647-2658.

[20] Kroutil, O.; Chval, Z.; Skelton, A. A.; Predota, M. (2015). Computer simulations of quartz (101)–water Interface over a range of pH values. The Journal of Physical Chemistry C, 119(17), 9274-9286.

[21] Berendsen, H. J. C.; Grigera, J. R.; Straatsma, T. P. (1987). The missing term in effective pair potentials. Journal of Physical Chemistry, 91(24), 6269-6271.

[22] Li, P.; Merz Jr, K. M. (2013). Taking into account the ion-induced dipole interaction in the nonbonded model of ions. Journal of Chemical Theory and Computation, 10(1), 289-297.

[23] Li, P.; Song, L. F.; Merz Jr, K. M. (2014). Parameterization of highly charged metal ions using the 12-6-4 LJ-type nonbonded model in explicit water. The Journal of Physical Chemistry B, 119(3), 883-895.

[24] Li, P.; Song, L. F.; Merz Jr, K. M. (2015). Systematic parameterization of monovalent ions employing the nonbonded model. Journal of Chemical Theory and Computation, 11(4), 1645-1657.
[25] Darden, T.; York, D.; Pedersen, L. (1993). Particle mesh Ewald: An N·log (N) method for Ewald sums in large systems. The Journal of Chemical Physics, 98(12), 10089-10092.
[26] Bussi, G.; Donadio, D.; Parrinello, M. (2007). Canonical sampling through velocity rescaling. The Journal of Chemical Physics, 126(1), 014101.

★★★